Final Report
New Jersey Space Grant Consortium
Summer Internship, Summer 2022

Impact-Induced Demagnetization in Martian Crust with High-Resolution MAVEN Data

By

Zain Eris Kamal
Department of Physics and Astronomy
Rutgers University
zain.eris.kamal@rutgers.edu

Advisor: Lujendra Ojha
Department of Earth and Planetary Sciences
Rutgers University
luju.ojha@rutgers.edu

Advisor Approval Signature: Lujendra Ojha

Advisor Approval Date: August 15, 2022

Abstract

A planet's dynamo is closely tied to the structure and evolution of its core, mantle, lithosphere, surface, and atmosphere. The Mars Global Surveyor (MGS) satellite mission (1996-2006) confirmed the absence of a presently active Martian dynamo, but further MGS analysis and studies of fragmented meteorites on Earth suggest the dynamo was active $\sim$ 4-Ga ago. However, the precise timing of the dynamo's demise is still debated, with estimates ranging from 4.2-Ga (Early Noachian era) to 3.6-Ga (Early Hesperian era). Impact craters offer a unique window into the dynamo's earliest history as they involve the sudden heating of iron-bearing minerals past their Curie point, introducing a thermoremanent magnetization that reflects the background magnetic field present at the time of cooling which can be preserved for billions of years. Here, we take a closer look at impact-induced magnetic anomalies with high-resolution magnetometer data from the NASA Mars Atmosphere and Volatile Evolution mission (MAVEN) orbiter. We analyze MAVEN data collected at nighttime and altitudes less than 200 km in/around all craters with diameters between 70-1,000 km, then contextualize the impact in Mars's geological history. Out of 857 total craters that fit these constraints, we find 24 that exhibit impact-induced demagnetization and 1 that uniquely exhibits possible remagnetization. Among these, 16 occurred in the Noachian era, 5 in the Hesperian era, and 4 in the Amazonian era, with the earliest instance of demagnetization occurring in the Early Noachian highland unit and the single instance of remagnetization occurring in the Middle Noachian highland unit. Our findings corroborate previous MGS analyses of impact-induced demagnetization, as well as suggest a lower limit for the Martian dynamo's demise in the Noachian period.

1. Introduction

1.1. History of the Martian Dynamo

At the present, stable liquid water can't exist on the surface of Mars due to its extremely thin and cold atmosphere. However, the presence of dried-up valley networks, sedimentary deposits, large flood channels, and polar ice caps provide compelling evidence that Mars used to have a rich, thick atmosphere that could support expansive bodies of surface water (Orosei et al., 2020).

Findings from the NASA Mars Atmosphere and Volatile EvolutioN (MAVEN) satellite orbiter mission (2014 - present) reveal that the Martian atmosphere was stripped away over time by solar wind, or highly energetic charged particles released from the upper atmosphere of the Sun (Sakata et al., 2020). However, this wasn't always the case — as is presently the case on Earth, Mars used to have an internal magnetic field that deflected solar wind and prevented atmospheric erosion.

The internal magnetic field of celestial bodies such as planets and stars is also called the dynamo. This occurs when

convection currents of rising/cooling molten metal in the body's core induce circulating electrical currents, which in turn induce a large-scale magnetic field that is aligned by the body's rotation about an axis. In addition to deflecting solar wind, the dynamo is closely tied to the structure and evolution of its core, mantle, lithosphere, surface, and atmosphere.

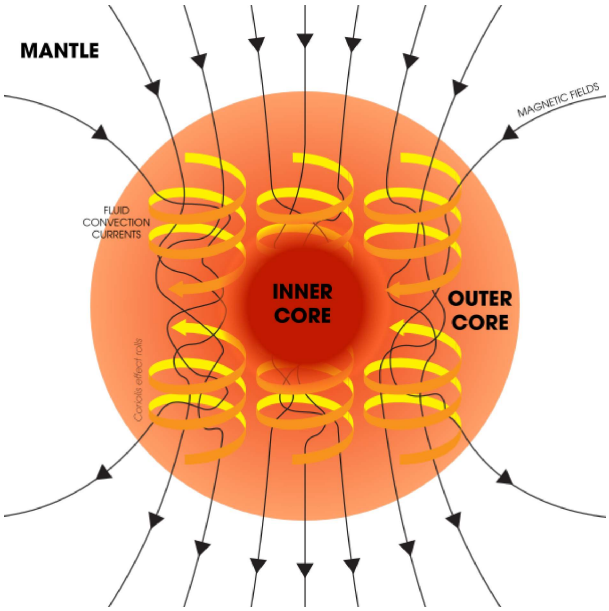

Figure 1: Illustration of the dynamo mechanism that creates large-scale planetary magnetic fields.

The NASA Mars Global Surveyor (MGS) satellite orbiter mission (1996 - 2006) confirmed the lack of a presently active Martian dynamo (Stevenson, 2001). However, studies of the fragmented meteorite ALH84001 show that the Martian dynamo was active until about 4 Ga (gigannums, or 4 billion years) ago (Weiss et al., 2002). The precise timing of the dynamo's demise is still debated, with estimates ranging from 4.2-Ga (Early Noachian era) to 3.6-Ga (Early Hesperian era). Many important geological events such as volcanism, major impact basins, and valley network activity occurred within this period, so a clearer picture of the dynamo's evolution/demise will help us understand and contextualize early geological activity.

1.2. Impact-Induced Demagnetization

Since certain minerals can preserve magnetization acquired by their planetary field for billions of years, studying them can give us a window into the planet's earliest conditions. Iron-bearing minerals that experience sudden shock wave pressures and are heated past a certain temperature called the Curie point can be demagnetized and acquire a thermoremanent magnetization (TRM) with direction/magnitude determined by the presence of a background magnetic field (i.e. the dynamo) as they cool (Mittelholz et al., 2020). Notably, meteorite impacts cause sudden demagnetization/TRM as opposed to the slow, enigmatic TRM of volcanic processes.

We expect the shock wave pressure produced by impacts that created craters of diameters 300—1,000 km to significantly demagnetize the underlying crust — however, a 2007 study of MGS data found only five instances of impact-induced demagnetization in craters of that size range (Shahnas & Arkani-Hamed, 2007).

In this work, we analyze high-resolution MAVEN magnetic field tracks in/around 857 craters of diameters 70—1,000 km to revisit previous interpretations of impact-induced demagnetization and ultimately shed light on the history of the Martian dynamo.

2. Methods

2.1. Data

The Mars Atmosphere and Volatile EvolutioN (MAVEN) satellite operated by NASA has been collecting data from Mars's orbit from 2014 to present day. MAVEN's magnetometers can measure the crustal magnetic field at altitudes as low as 130 km with high resolution, allowing us to detect signals that were too weak or had wavelengths too short to be observed by MGS. Additionally, global nighttime data at altitudes under 200 km cover 93% of Mars as opposed to the <20% coverage of MGS.

Vector magnetic field data acquired by the Fluxgate Magnetometers aboard the MAVEN spacecraft can be downloaded from the NASA Planetary Data System website. We use data collected at nighttime (20:00—09:00) and altitudes less than 200 km. This is because solar radiation induces electric currents in Mars's ionosphere which generate their own magnetic fields, introducing longwave biases that muddle and intensify MAVEN's measurements of sunny terrain. The original dataset is about 1.2 TB, but removing measurements that don't fit these constraints with the script reduce_MAVEN_MAG.m brings the dataset down to $\sim$ 10 GB, significantly increasing processing speed.

For crater locations, we use a comprehensive global database of Mars impact craters $\geq$ 1 km in diameter (Robbins & Hynek, 2012). We extract the coordinates for craters with diameters between 70—1,000 km, which comes out to 857 total craters.

2.2. Analysis

Our analysis is performed within the script generate_crater_shapefiles_v2.m. For each crater we isolate MAVEN measurements taken inside the crater, separate the individual tracks, and then extend these tracks by ten times the crater radius in the plus and minus latitude directions. We then plot the following six components as a function of latitude with/without linear detrending (where we subtract each track's best fit linear regression line):

- Bottom row: B_r, B_θ, and B_ϕ (vector components of the magnetic field in spherical coordinates),
- Top row: $|B|$ (magnitude of the magnetic field), $||B||$ (magnitude of the magnetic field where each track is individually normalized by its max value), and Altitude (of the MAVEN satellite at the time of measurement).

The solid and dashed lines represent the crater radius and 1.5x the crater radius respectively.

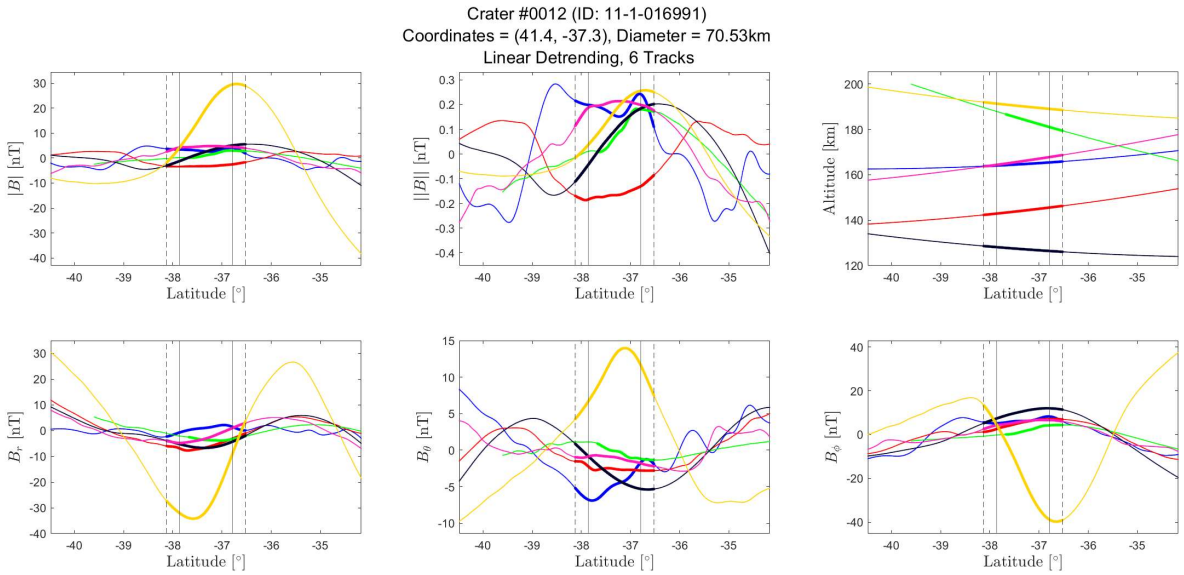

Figure 2: Magnetic signatures surrounding an unnamed crater. The "flatness" of the $|B|$ plot indicates the absence of any impact-induced magnetic anomalies at this crater. The yellow track appears to be an outlier, but its relatively higher altitude gives us some confidence in discarding it as noise.

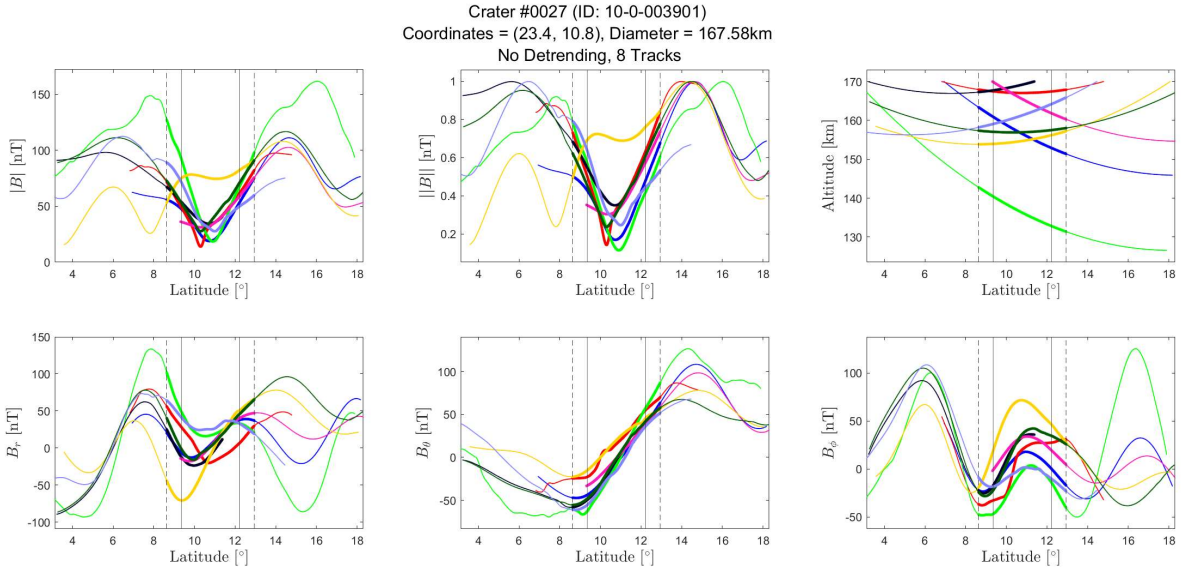

Figure 3: Magnetic signatures surrounding Henry crater. The strong "dip" in $|B|$ and $||B||$ as the tracks pass through the crater suggest strong impact-induced demagnetization by more than 80% of the original field. Additionally, there was enough data in this crater to reduce the maximum altitude from 200 km to 170 km, further increasing the resolution and confidence in our results.

At this point, we can go through all of the craters and find promising examples where the tracks are both coherent and suggest some kind of magnetic anomalies. For these, we convert all magnetic field data surrounding the crater (not just data belonging to tracks that pass through the crater) to shapefiles for visualization with QGIS.

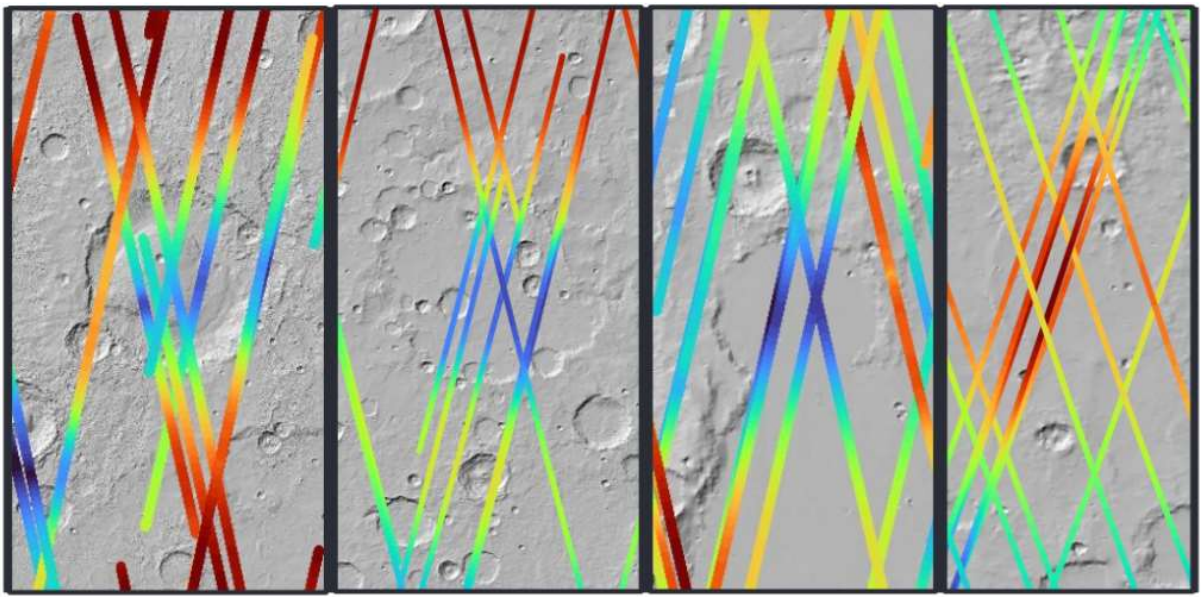

Figure 4: Some compelling examples of impact-induced magnetic anomalies. The tracks represent $||B||$, where blue indicates a value of ~ 0 and red indicates a value of 1. The first three craters exhibit demagnetization, whereas the rightmost crater uniquely exhibits *re*magnetization.

This is less quantitative than the cross-sectional line plots, but still necessary to ensure we're not misinterpreting a longitudinal strip of magnetization that happens to coincide with a crater as an impact-induced anomaly.

With our final candidates of impact-induced magnetic anomalies, we attempt to find when in Mars's geological history the impact occurred. This is done with a GIS database of Martian surface features dated in the Noachian, Hesperian, and Amazonian periods (Tanaka et al., 2014).

2.3. Code/Data Availability

The processed data used in our analysis and MATLAB code used to generate it is available in this GitHub repository.

---

3. Conclusions

3.1. Results

Out of 857 total craters with diameters between 70—1,000 km, we found 24 that exhibit impact-induced demagnetization and 1 that uniquely exhibits possible remagnetization. Among these, 16 occurred in the Noachian era, 5 in the Hesperian era, and 4 in the Amazonian era, with the earliest instance of demagnetization occurring in the Early Noachian highland unit and the single instance of remagnetization occurring in the Middle Noachian highland unit.

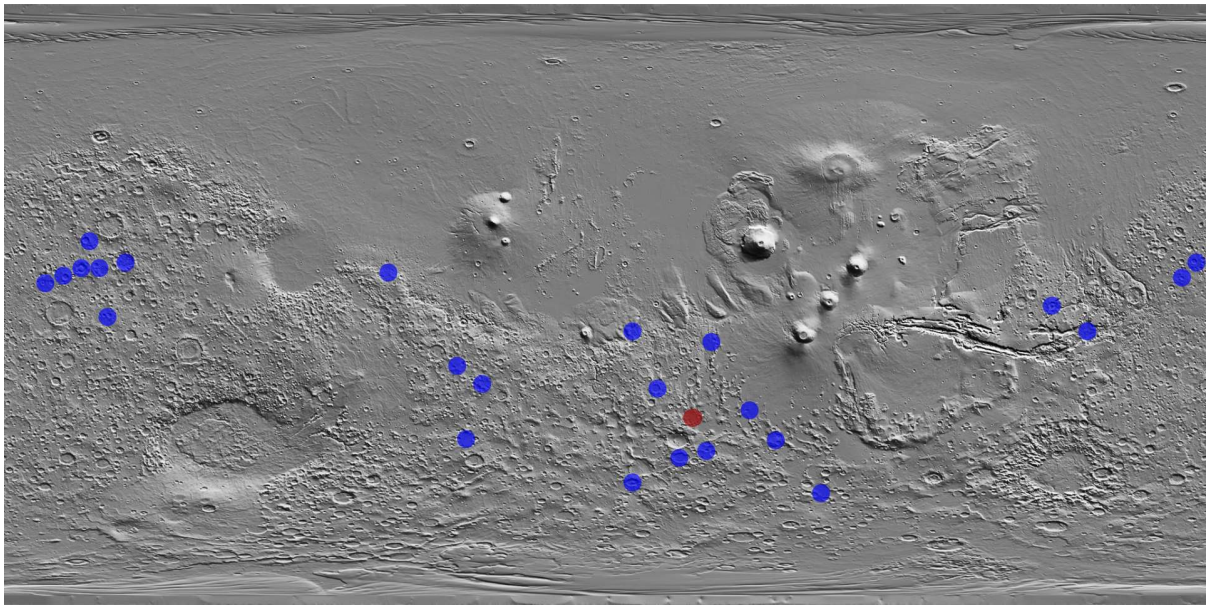

Figure 5: Global map of Mars with impact-induced demagnetization sites labeled in blue and remagnetization labeled in red.

Our findings corroborate previous MGS analyses of impact-induced demagnetization (Shahnas & Arkani-Hamed, 2007), as well as suggest a lower limit for the Martian dynamo's demise in the Noachian period, supporting the "Early dynamo" hypothesis.

3.2. Future Work

The reason behind the rarity of impact-induced magnetic anomalies is unclear. We notice a clustering of magnetic anomalies in a large upland region in the north of Mars known as Arabia Terra (see top left of Figure 5) which lies in a transitionary region between high/low elevations, and also contains a well-studied impact site called Henry crater (signatures shown in Figure 3). We plan to take a closer look at that region while considering extra geophysical parameters such as crustal thickness and sediment deposits to better understand why that specific region has so many instances of impact-induced demagnetization.

Future work also includes using Alain Plattner's vector Slepian functions toolkit (Plattner & Simons, 2015) to produce
high-resolution local spherical harmonic models around craters to better understand field variations, remove noise, and isolate upper-crust magnetic field contributions. We can also look at the cumulative sub-crater density within a crater to find its age with greater resolution.

4. References

Hynek, B. M., Beach, M., & Hoke, M. R. T. (2010). Updated global map of Martian valley networks and implications for climate and hydrologic processes. *Journal of Geophysical Research: Planets*, *115*(E9).

Mittelholz, A., Johnson, C. L., Feinberg, J. M., Langlais, B., & Phillips, R. J. (2020). Timing of the martian dynamo: New constraints for a core field 4.5 and 3.7 Ga ago. *Science Advances*, *6*(18), eaba0513.

Orosei, R., Ding, C., Fa, W., Giannopoulos, A., Hérique, A., Kofman, W., et al. (2020). The Global Search for Liquid Water on Mars from Orbit: Current and Future Perspectives. *Life*, *10*(8), 120. https://doi.org/10.3390/life10080120

Plattner, A., & Simons, F. J. (2015). High-resolution local magnetic field models for the Martian South Pole from Mars Global Surveyor data. *Journal of Geophysical Research: Planets*, *120*(9), 1543–1566.

Robbins, S. J., & Hynek, B. M. (2012). A new global database of Mars impact craters ≥1 km: 1. Database creation, properties, and parameters. *Journal of Geophysical Research: Planets*, *117*(E5).

Sakata, R., Seki, K., Sakai, S., Terada, N., Shinagawa, H., & Tanaka, T. (2020). Effects of an Intrinsic Magnetic Field on Ion Loss From Ancient Mars Based on Multispecies MHD Simulations. *Journal of Geophysical Research: Space Physics*, *125*(2). https://doi.org/10.1029/2019ja026945

Shahnas, H., & Arkani-Hamed, J. (2007). Viscous and impact demagnetization of Martian crust. *Journal of Geophysical Research: Planets*, *112*(E2).

Stevenson, D. J. (2001). Mars' core and magnetism. *Nature*, *412*(6843), 214–219. https://doi.org/10.1038/35084155

Tanaka, K. L., Robbins, S. J., Fortezzo, C. M., Skinner, J. A., & Hare, T. M. (2014). The digital global geologic map of Mars: Chronostratigraphic ages, topographic and crater morphologic characteristics, and updated resurfacing history. *Planetary and Space Science*, *95*, 11–24.

Weiss, B. P., Vali, H., Baudenbacher, F. J., Kirschvink, J. L., Stewart, S. T., & Shuster, D. L. (2002). Records of an ancient Martian magnetic field in ALH84001. *Earth and Planetary Science Letters*, *201*(3–4), 449–463. https://doi.org/10.1016/s0012-821x(02)00728-8